Electronic Supplementary Material (ESI) for Journal of Materials Chemistry A.

Simultaneous improvement of efficiency and stability of inverted organic solar cell via composite hole transport layer

Qiri Huang, Jianhua jing, Kai Zhang*, Yanwei Chen, Ao Song, Zixian Liu, Fei Huang*

Institute of Polymer Optoelectronic Materials and Devices, State Key Laboratory of Luminescent Materials and Devices, South China University of Technology, Guangzhou 510640, P. R. China.

**Corresponding author*

E-mail: mszhangk@scut.edu.cn; msfhuang@scut.edu.cn.

Experimental Section

Materials

PM6 and L8-BO-F were purchased from Solarmer Materials Inc. Y6-BO was purchased from Dethon Optoelectronics Materials Co.,LTD. 2PCAz was purchased from Tokyo Chemical Industry (TCI) Co., LTD. All materials and solvents were commercially available and used as received.

Devices Fabrication

The devices were fabricated with inverted structures of ITO/AZO/PM6:L8-BO-F:Y6-BO/2PACz/MoO_3 (10 nm)/Ag (100 nm) and ITO/AZO/PM6:L8-BO-F:Y6-BO/2PACz or MoO_3 (10 nm)/Ag (100 nm). The patterned indium tin oxide (ITO) glass substrates were cleaned sequentially by sonication with deionized water and isopropanol, and then dried at 65℃ in a baking oven overnight. After UV-ozone treatment for 4 min, and then coated with AZO at 2500 rpm for 30 s. After annealing in air at 150 °C on a hot plate for 15 min, the substrates were transferred into a nitrogen-filled protected glove box. Sequentially, the active layer solution of PM6:L8-BO-F:Y6-BO (1:0.2:1.2, w/w, dissolved by CF:DIO = 99.5:0.5, v/v, with a total concentration of 15.4 mg ml^{-1}) was spin-coated at 3000 rpm with the optimal thickness of 110 nm onto the AZO. Then the active layers were thermally annealed at 100 ℃ for 10 min. For 2PACz-modified cells, different concentrations 2PACz ethanol solution were prepared (0.25 mg/ml, 0.5 mg/ml, 1 mg/ml and 2 mg/ml respectively). 2PACz ethanol solution were spin-coated at 3000 rpm onto the active layers to attain different thickness. Then, the active layers with 2PACz were thermally annealed at 100 ℃ for 10 min. Finally, 10 nm of MoO_3 and 100 nm Ag were thermally deposited on top of all devices through a mask under a vacuum of ~1×10^{-7} mbar. The effective area of the devices was 0.04 cm^2.

Instruments and Measurement

J-V and EQE: The current density-voltage (*J-V*) characteristics of the devices were measured under 1 sun, AM 1.5 G solar simulator (Taiwan, Enlitech SS-F5) by using a computer-controlled Keithley 2400 Source Meter. The light intensity was calibrated by a China General Certification Center (CGC) certified reference silicon solar cell (Enlitech) before test, giving a 100 mW cm^{-2} light intensity during test. The external quantum efficiency (EQE) data were recorded with a QE-R test system (Enlitech).

UV-vis absorption spectra: UV-vis spectra were recorded on a SHIMADZU UV-3600 spectrophotometer from 300 to 1000 nm, corrected for quartz absorption.

Morphology characterizations: AFM images were tested by a Digital Instrumental DI Multimode Nanoscope III in a taping mode. TEM imagines were tested by a JEM-2100F instrument. The cross-section TEM imaging was prepared by an FEI STRATA 400S focused in the beam-scanning electron microscope, and cross-section TEM patterns and EDS data were recorded in FEI Talos F200s super-X TEM operated at 200 kV.

Built-in potential measurement: The Mott-Schottky characteristics were measured by the keysight E4990A Vector Network Analyzer with a voltage range of -3 to 2 V under dark conditions. The performance of the devices was tested both before and after the measurements with no sign of degradation.

Electrochemical impedance spectroscopy measurement: The impedance characteristics were measured by the keysight E4990A Vector Network Analyzer with the frequency measurement range of 1 Hz to 10 MHz under dark conditions. The performance of the devices was tested both before and after the measurements with no sign of degradation.

TPC and TPV Measurements: The transient photocurrent and transient photovoltage characteristics of devices were measured by applying 500 nm laser pulses with a pulse width of 120 fs and a low pulse energy to the short-circuit devices in the dark. The laser pulses were generated from an optical parametric amplifier (TOPAS-Prime) pumped by a mode-locked Ti: sapphire oscillator seeded regenerative amplifier with a pulse

energy of 1.3 mJ at 800 nm and a repetition rate of 1 kHz (Spectra Physics Spitfire Ace). The charge extraction time was extracted from the fitting line of the TPC signal with the equation: $\delta I = A\exp(t/T)$, where A is a constant that fits the peak high, t is time, and T is the charge extraction time. The transient photovoltage was tested under the open-circuit condition to explore the photovoltage decay. The photovoltage decay kinetics of all devices follow a mono-exponential decay: $\delta V = A\exp(-t/T)$ where t is the time, and T is the charge carrier lifetime.

The CE measurement was used to measure the charge carrier density n under open-circuit voltage conditions. The device was illuminated and kept at open circuit. After the light was turned off, the voltage was set to zero or taken to short-circuit condition within a few hundred nanoseconds to extract the charges. To obtain the number of extracted charges, the current was integrated. Using the charge carrier lifetime obtained from TPV and charge carrier density from CE, the charge carrier lifetimes and charge carrier densities can be plotted. The charge carrier lifetime follows a power-law relationship with charge density: $\tau = \tau_0\ n^{-\lambda}$. The nongeminate recombination constant k_{rec} was then inferred from the carrier lifetimes and densities according to $k_{rec} = 1/(\lambda + 1)n\tau$, where λ is the recombination order determined from Figure S8c.

Space charge limited current (SCLC) measurements: The hole-only devices were fabricated with the structure of ITO/PEDOT:PSS/BHJ or PM6/2PACz/MoO_3/Ag and ITO/PEDOT:PSS/BHJ or PM6/MoO_3/Ag to evaluate the hole mobility and injection property. Hole-only devices were recorded with a Keithley 236 sourcemeter under dark. The hole mobility was determined by fitting the dark current based on a single-carrier SCLC model, which is described by the equation:

$$J = \frac{9}{8}\varepsilon_0\varepsilon_r\mu\frac{V^2}{d^3},$$

where J is the current density, μ is the zero-field mobility, ε_0 is the permittivity of free space, ε_r is the relative permittivity of the material, d is the thickness of the BHJ or PM6, and V is the effective voltage. The effective

voltage (V_{eff}) was obtained by subtracting the built-in voltage ($V_{bi} = 0$) and the voltage drop ($V_s = 10 \times I$, where the value 10 is the resistance of MoO_3, and I is the current of the devices in this work) from the applied voltage (V_{appl}), $V = V_{appl} - V_{bi} - V_s$. The hole mobility can be calculated from the slope of the $J^{1/2}$-V curves.

Light operational stability measurements: The devices were encapsulated with epoxy glue and glass in N_2 protected box. Then the devices were transferred into atmosphere, where the temperature was around 25 ℃ and humidity between 50-60%, for the stability test. Light exposure was performed using a LED source with light intensity calibrated to achieve the same device performance measured by the standard AM 1.5 G solar simulator.

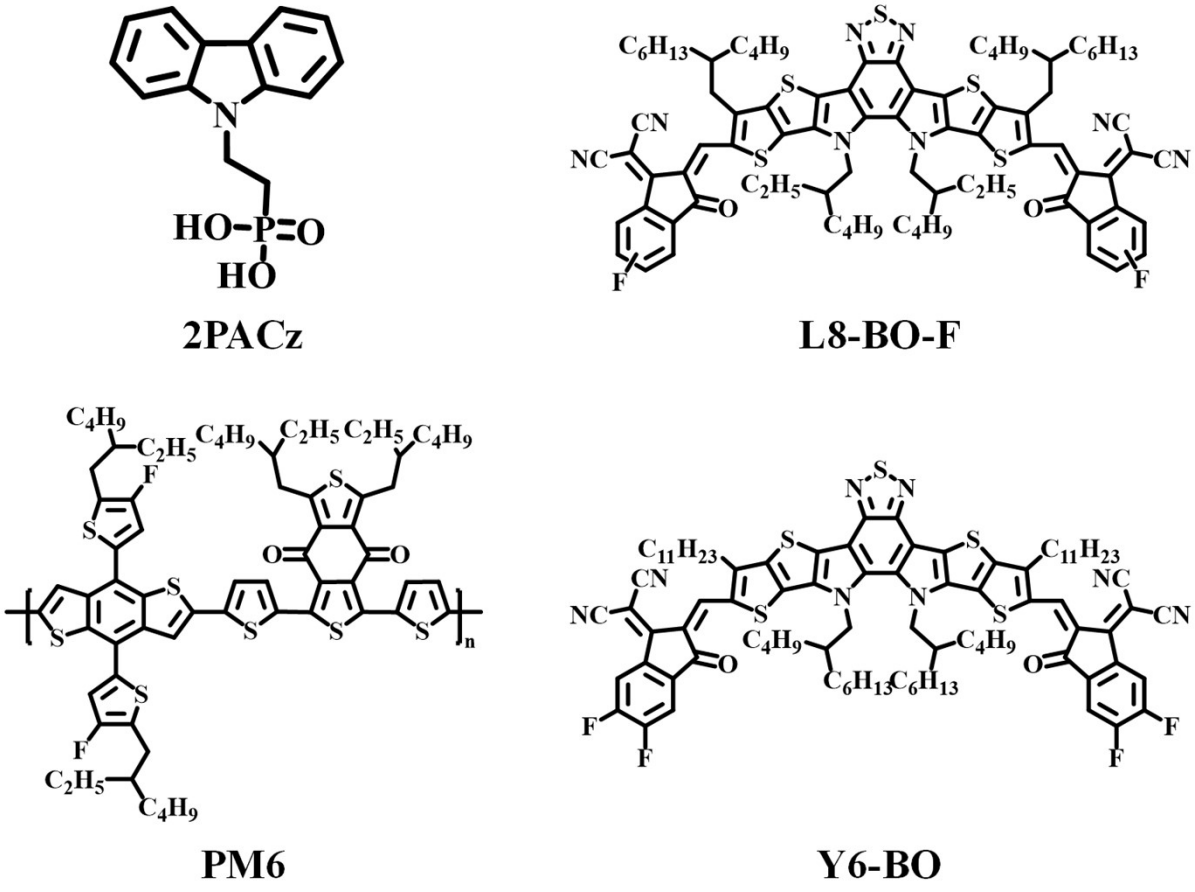

Figure. S1. Molecular structures of BHJ and 2PACz materials.

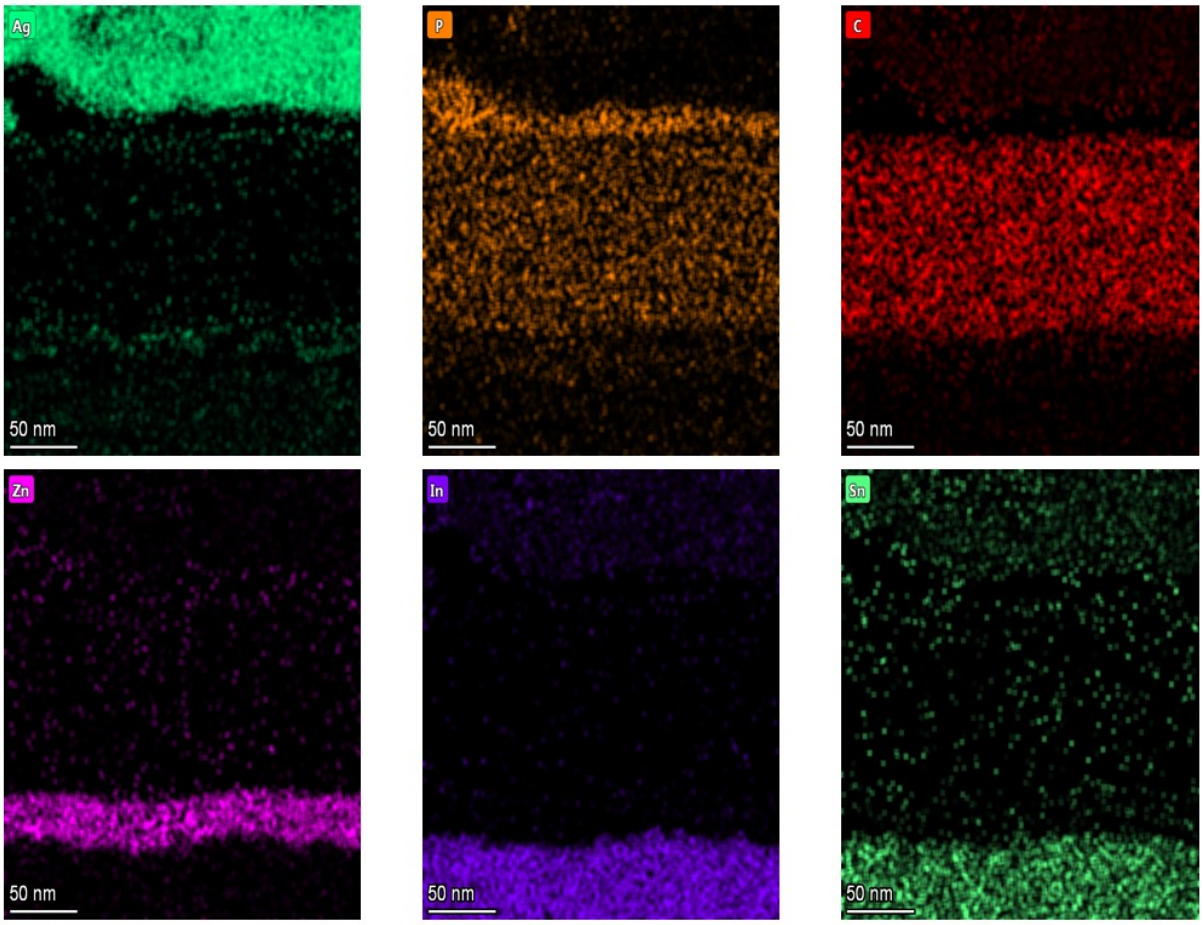

Figure. S2. Mapping images of the six elements distribution of the prepared device.

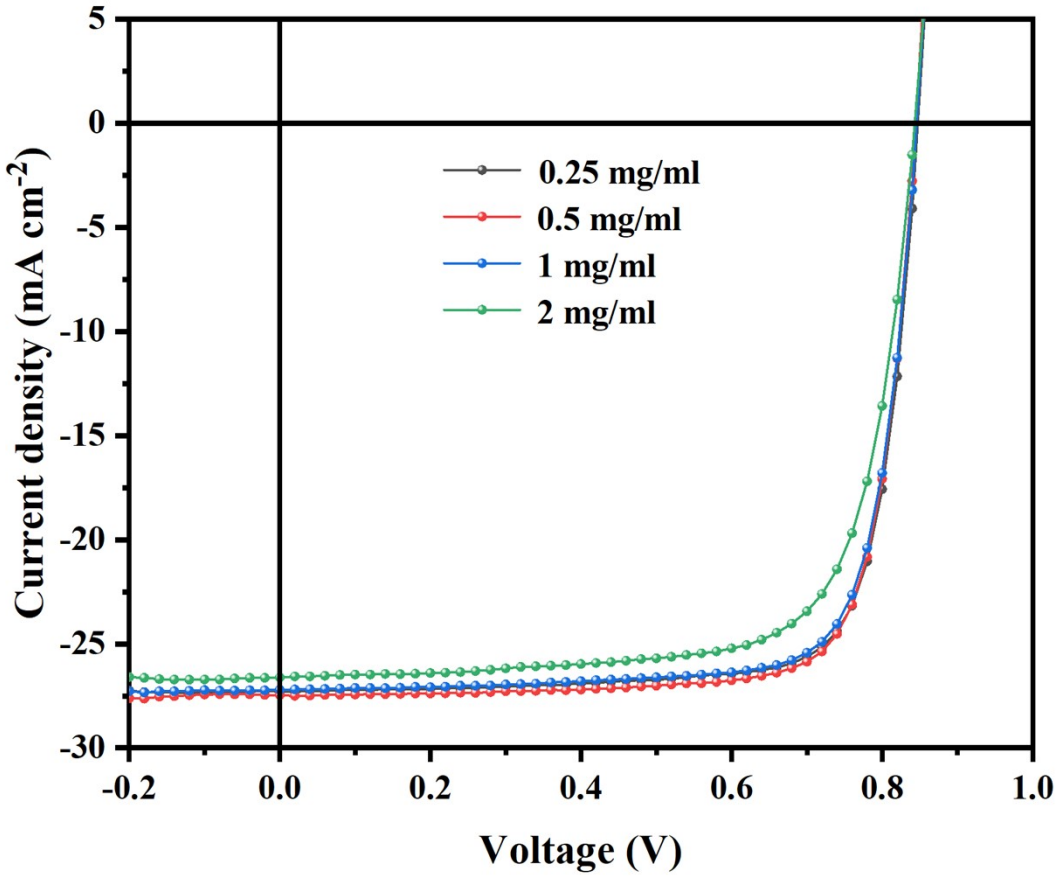

Figure. S3. *J-V* curve of devices with different concentrations of 2PACz.

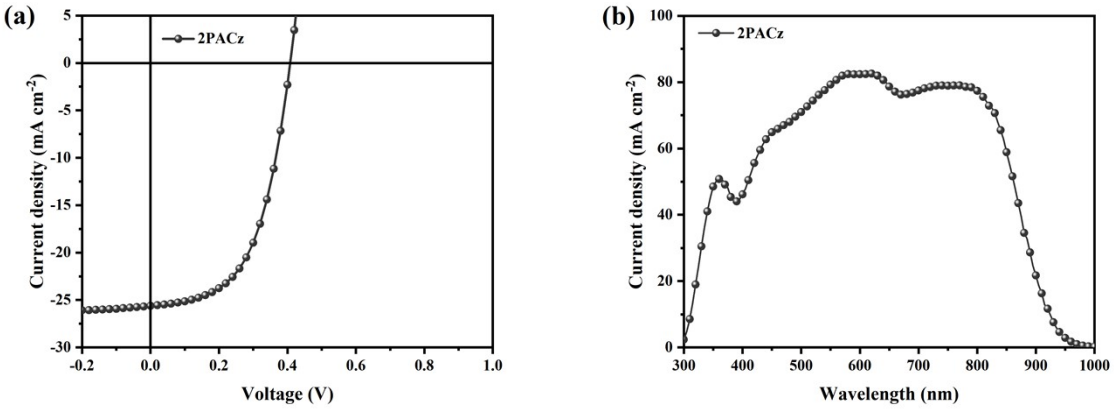

Figure. S4. (a) *J-V* curve of the 2PACz-based device. (b) EQE curve the 2PACz-based device.

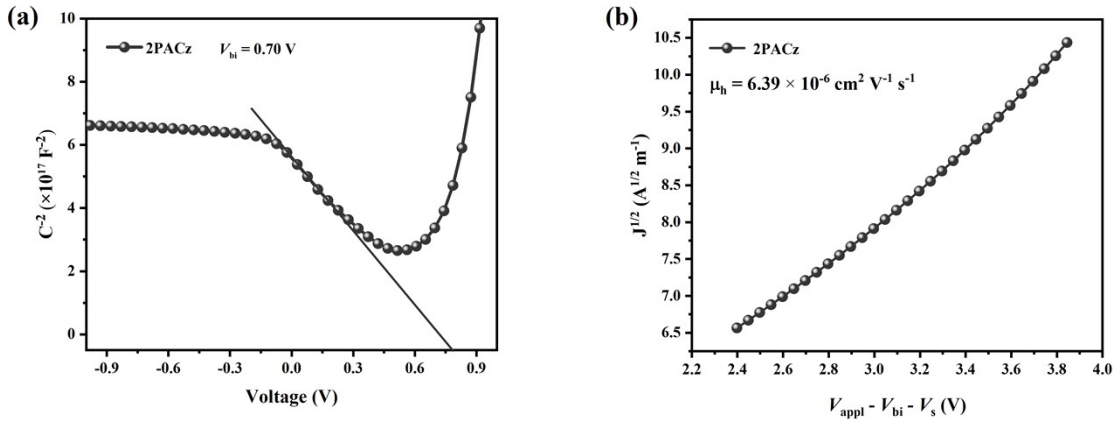

Figure. S5. (a) Mott-Schottky characteristics of the 2PACz-based device. (b) Hole mobility curves of device based on 2PACz HTL.

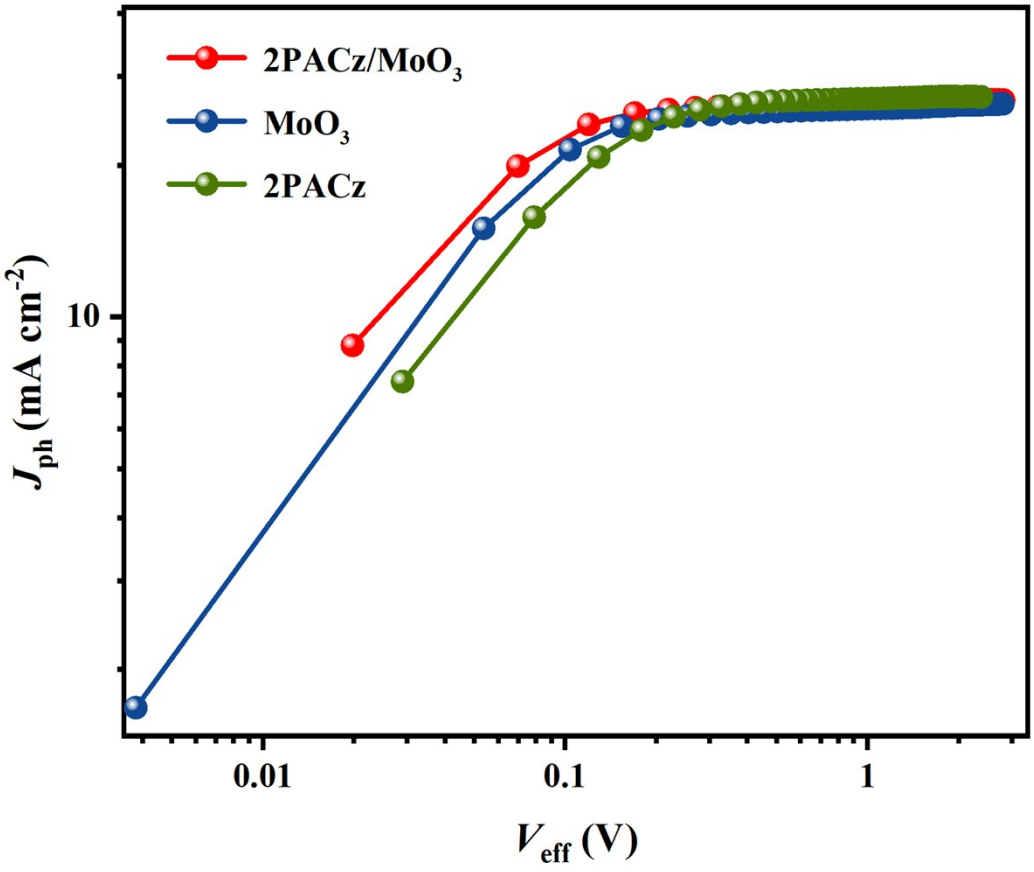

Figure. S6. J_{ph}-V_{eff} plot of the three devices.

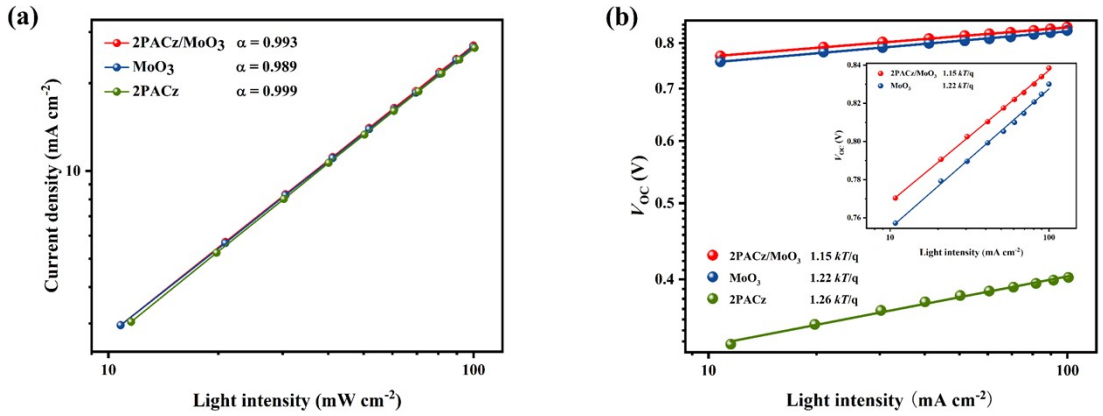

Figure. S7. (a) Light intensity dependence of J_{SC}. (b) Light intensity dependence of V_{OC}.

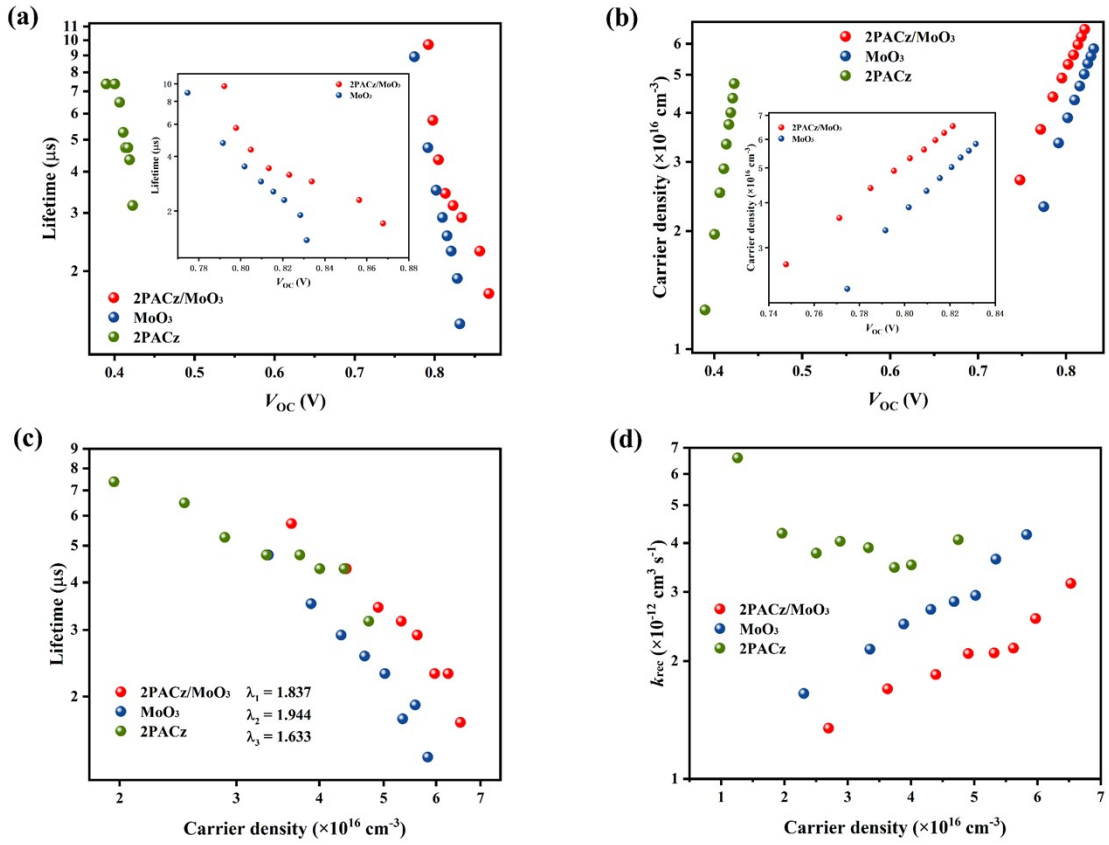

Figure. S8. (a) The carrier lifetime as a function of V_{OC} under different bias light intensities. (b) The extracted carrier density under different open circuit conditions. (c) Carrier lifetime as a function of the carrier density. (d) Recombination rate coefficients (k_{rec}) for the solar cells.

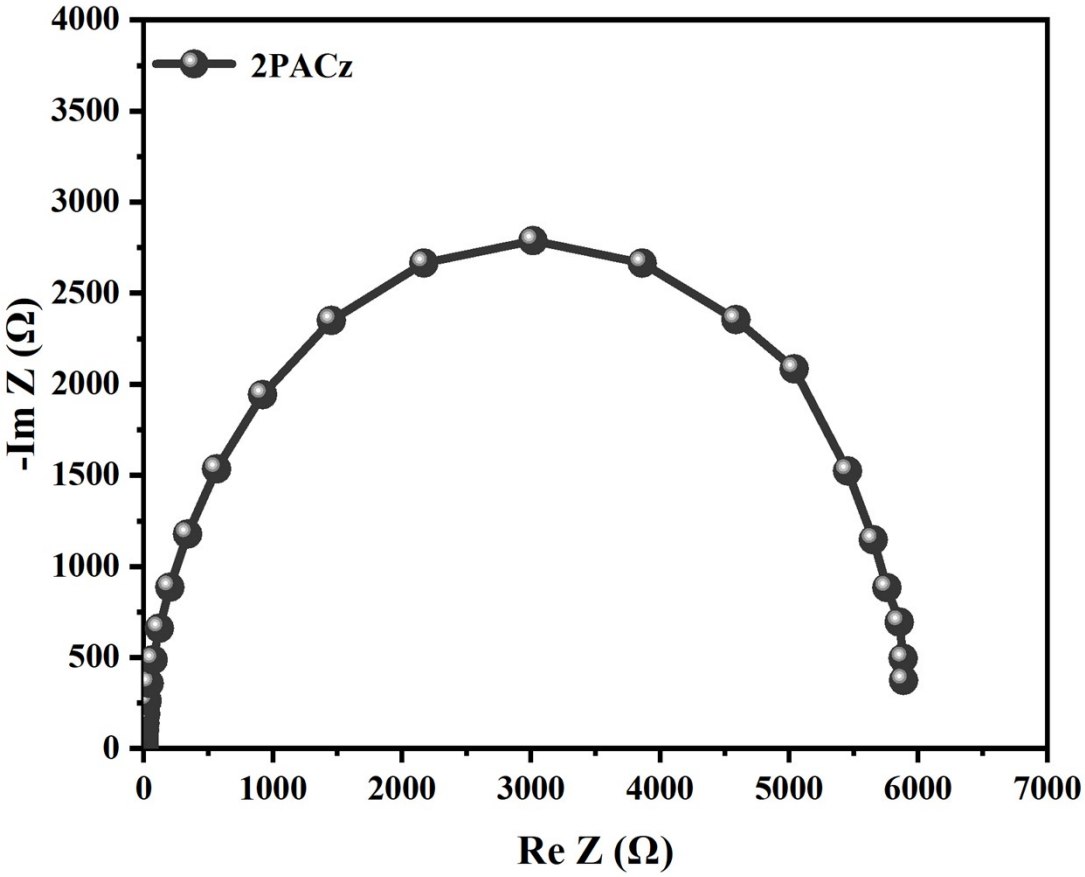

Figure. S9. The impedance spectrum of 2PACz-based device at the open circuit voltage condition under dark conditions.

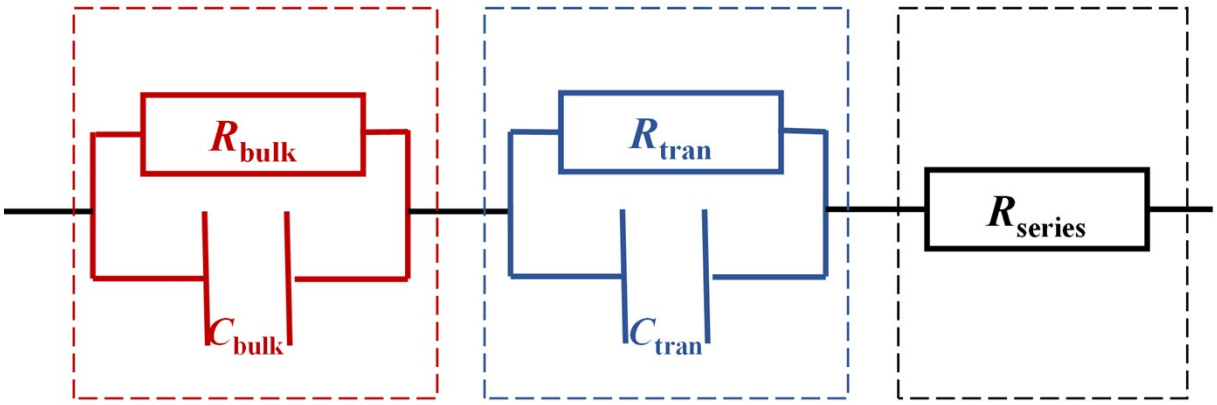

Figure. S10. Diagram of the equivalent-circuit model.

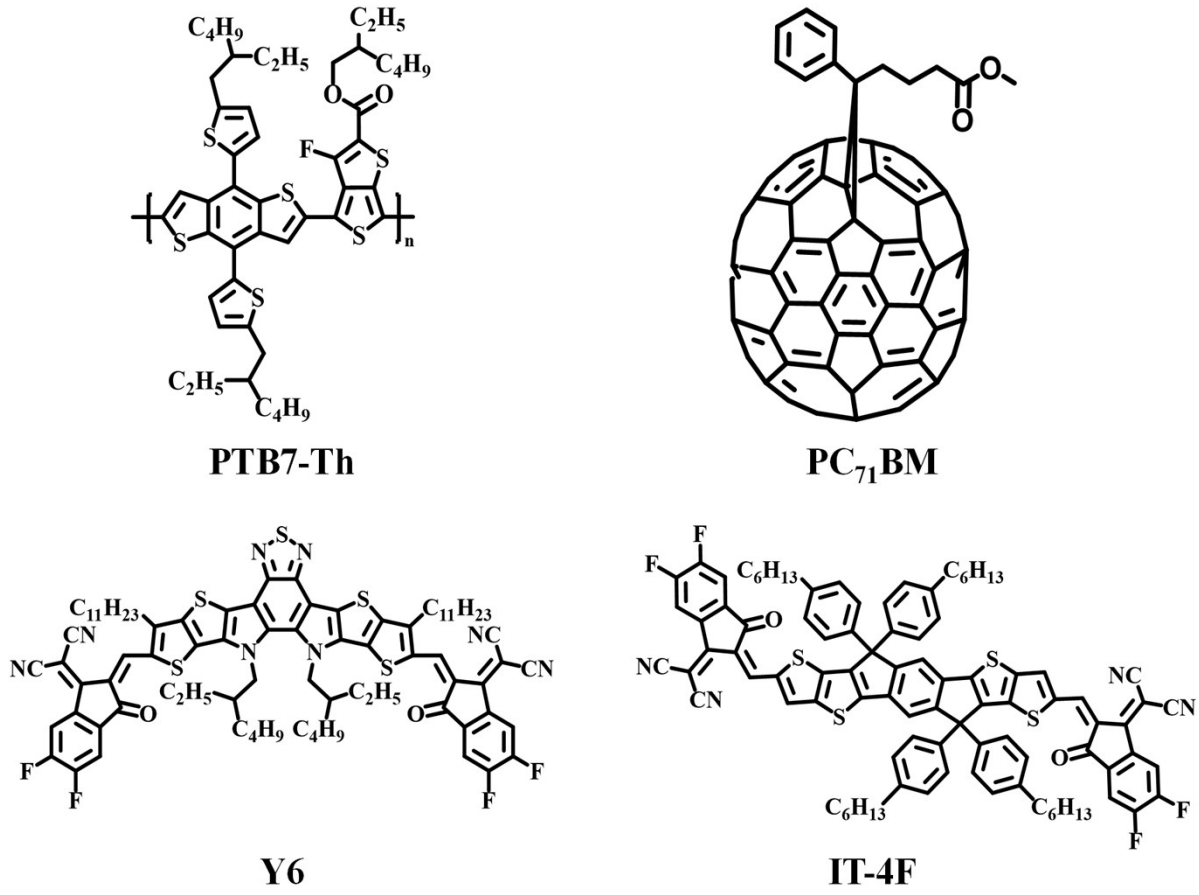

Figure. S11. Molecular structures of PTB7-Th, $PC_{71}BM$, Y6 and IT-4F.

Table S1. Summary of the device characteristics based on ITO/AZO/PM6:L8-BO-F:Y6-BO/2PACz/MoO_3/Ag with different concentrations of 2PACz.

2PACz (mg ml^{-1})	V_{OC} [V]	J_{SC} [mA cm^{-2}]	FF [%]	PCE [%]
0.25	0.85	27.06	78.73	18.11
0.5	0.85	27.41	79.68	18.49
1	0.85	27.08	77.91	17.93
2	0.84	26.62	73.74	16.49

Table S2. Summary of the parameters used to describe the J_{ph}-V_{eff} plot based on ITO/AZO/PM6:L8-BO-F:Y6-BO/HTLs/Ag.

HTLs	V_0 (V)	J_{sat} (mA cm^{-2})	J_{ph} (mA cm^{-2})	G_{max} (m^{-3} s^{-1})	P(E,T) (%)	L (nm)
2PACz/MoO_3	0.829	26.97	26.50	1.53×10^{28}	98.27	110
MoO_3	0.804	26.50	25.81	1.50×10^{28}	97.40	110
2PACz	0.380	27.64	26.75	1.57×10^{28}	96.77	110

Table S3. Summary of the fitting parameter used to describe the impedance spectrum.

HTLs	R_{bulk} (Ω)	R_{tran} (Ω)	R_{series} (Ω)
2PACz/MoO_3	848	24.2	4.69
MoO_3	1040	123	8.36
2PACz	6390	32.8	4.41

Table S4. Device photovoltaic parameters based on MoO_3 and 2PACz/MoO_3 HTL in different BHJ.

BHJ	HTLs	V_{OC} [V]	J_{SC} [mA cm^{-2}]	FF [%]	PCE [%]
PM6:Y6	2PACz/MoO_3	0.83±0.00 (0.83)	26.93±0.12 (27.02)	74.54±0.72 (75.05)	16.49±0.34 (16.83)
	MoO_3	0.82±0.00 (0.82)	26.71±0.17 (26.86)	72.97±1.10 (73.95)	15.94±0.32 (16.29)
PM6:Y6-BO	2PACz/MoO_3	0.83±0.00 (0.83)	26.84±0.31 (27.08)	77.31±0.69 (78.03)	17.10±0.26 (17.47)
	MoO_3	0.82±0.00 (0.82)	26.54±0.16 (26.64)	75.74±0.93 (76.46)	16.39±0.34 (16.70)
PM6:IT-4F	2PACz/MoO_3	0.81±0.00 (0.81)	20.72±0.37 (21.15)	74.47±0.26 (74.51)	12.45±0.25 (12.76)
	MoO_3	0.80±0.00 (0.80)	20.48±0.13 (20.67)	73.52±0.13 (73.60)	12.04±0.11 (12.17)
PTB7-Th:$PC_{71}BM$	2PACz/MoO_3	0.79±0.00 (0.79)	16.52±0.22 (16.86)	70.11±0.51 (71.14)	9.09±0.19 (9.46)
	MoO_3	0.78±0.00 (0.78)	16.20±0.32 (16.61)	69.70±0.48 (70.45)	8.86±0.22 (9.13)

Table S5. PCE summary of the representative inverted OSCs based on thermally evaporated MoO_3 HTL or composite HTL.

Year	**Structures**	**BHJ**	**PCE (%)**	**Ref.**
2022	ITO/ZnO/BHJ/MoO_3/Ag	PM6:Y6	15.03	[1]
2021	ITO/ZnO/PET/BHJ/MoO_3/Ag	PM6:Y6	16.46	[2]
2022	ITO/SnO2:PAS/BHJ/MoO_3/Ag	PM6:Y6	16.37	[3]
2020	ITO/OSiNDs/BHJ/MoO_3/Ag	PM6:Y6:PC71BM	17.15	[4]
2020	ITO/ZnO/BHJ/MoO_3/Ag	PM6:Y6:PC71BM	16.63	[4]
2022	ITO/CD/BHJ/MoO_3/Ag	PM6:Y6:PC71BM	16.80	[5]
2022	ITO/CD/BHJ/MoO_3/Ag	PM6:BTP-eC9	17.35	[5]

2022	ITO/SnO2/1-DPAQ/BHJ/MoO_3/Ag	PM6:BTP-eC9	17.7	[6]
2022	ITO/SnO2/1-DPAQ/BHJ/MoO_3/Ag	PM6:PB2F:BTP-eC9	18.1	[6]
2021	ITO/ZnO:Zr/BHJ/MoO_3/Ag	PM6:BTP-eC9	17.7	[7]
2021	ITO/PA-ZnO/BHJ/MoO_3/Ag	PM6:BTP-eC9	17.6	[8]
2022	ITO/SnO2:PAS/BHJ/MoO_3/Ag	PM6:BTP-eC9	17.12	[3]
2022	ITO/ZnO/BHJ/MoO_3/Ag	PM6:N3	15.00	[1]
2022	ITO/ZnO/BHJ/MoO_3/Ag	PM6:ITIC	10.28	[1]
2022	ITO/ZnO/PET/BHJ/MoO_3/Ag	PM6:L8-BO	17.02	[1]
2022	ITO/ZnO/BHJ/MoO_3/Ag	PM6:IT-4F	11.18	[1]
2019	ITO/ZnO:PFN-br/BHJ/MoO_3/Ag	PBDB-TF:IT-4F	13.82	9
2018	ITO/PVP/BHJ/MoO_3/Ag	PBDB-TF:IT-4F	13.3	10
2014	ITO/ZnO/CsSt/BHJ/MoO_3/Ag	PTB7:$PC_{71}BM$	8.69	11
2019	ITO/PFN/BHJ/DPA2T/MoO_3/Ag	PTB7:$PC_{71}BM$	9.32	12
2018	ITO/PEI/BHJ/PEDOT:PSS/MoO_3/Ag	PTB7:$PC_{71}BM$	9.54	13
2017	ITO/TiO_2/BHJ/$CuBr_2$/MoO_3/Ag	PTB7:$PC_{71}BM$	9.56	14
2017	ITO/PEIE/BHJ/MoO_3/PEIE/Ag	PTB7-Th:$PC_{71}BM$	8.42	15
2016	ITO/ZnO-NPs/BHJ/PEDOT:PSS/MoO_3/Ag	CdSe:P3HT	1.53	16
2020	ITO/PEIE/BHJ/CPB:MoO_3/ NPB:MoO_3/Ag	P3HT:PCBM	2.38	17
2012	ITO/ZnO/BHJ/MTDATA/MoO_3/Ag	PDTS-BTD:$PC_{71}BM$	6.45	18
2022	ITO/AZO/BHJ/2PACz/MoO_3/Ag	PM6:L8-BO-F:Y6-BO	**18.49**	**This work**

References

1 B. Liu, X. Su, Y. Lin, Z. Li, L. Yan, Y. Han, Q. Luo, J. Fang, S. Yang, H. Tan and C. Q. Ma, *Adv. Sci.*, 2022, **9**, 2104588.

2 Y. Han, H. Dong, W. Pan, B. Liu, X. Chen, R. Huang, Z. Li, F. Li, Q. Luo, J. Zhang, Z. Wei and C. Q. Ma, *ACS Appl. Mater. Interfaces*, 2021, **13**, 17869-17881.

3 H. Gao, X. Wei, R. Yu, F. Y. Cao, Y. Gong, Z. Ma, Y. J. Cheng, C. S. Hsu and Z. a. Tan, *Adv. Opt. Mater.*, 2022, **10**, 2102031.

4 M. Cui, D. Li, X. Du, N. Li, Q. Rong, N. Li, L. Shui, G. Zhou, X. Wang, C. J. Brabec and L. Nian, *Adv. Mater.*, 2020, **32**, e2002973.

5 Y. Dong, R. Yu, B. Zhao, Y. Gong, H. Jia, Z. Ma, H. Gao and Z. Tan, *ACS Appl. Mater. Interfaces*, 2022, **14**, 1280-1289.

6 R. Yu, X. Wei, G. Wu, T. Zhang, Y. Gong, B. Zhao, J. Hou, C. Yang and Z. a. Tan, *Energy Environ. Sci.*, 2022, **15**, 822-829.

7 X. Song, G. Liu, P. Sun, Y. Liu and W. Zhu, *J. Phys. Chem. Lett.*, 2021, **12**, 10616-10621.

8 X. Liu, Z. Zheng, J. Wang, Y. Wang, B. Xu, S. Zhang and J. Hou, *Adv. Mater.*, 2022, **34**, e2106453.

9 Z. Zheng, S. Zhang, J. Wang, J. Zhang, D. Zhang, Y. Zhang, Z. Wei, Z. Tang, J. Hou and H. Zhou, *J. Mater. Chem. A.*, 2019, **7**, 3570-3576.

10 B. Yang, S. Zhang, S. Li, H. Yao, W. Li and J. Hou, *Adv. Mater.*, 2019, **31**, e1804657.

11 G. Wang, T. Jiu, G. Tang, J. Li, P. Li, X. Song, F. Lu and J. Fang, *ACS Sustain. Chem. Eng.*, 2014, **2**, 1331-1337.

12 Y. Jiang, H. Peng, R. Mai, Y. Meng, Q. Rong, C. Cabanetos, L. Nian, J. Roncali, G. Zhou, J. Liu and J. Gao, *Org. Electron.*, 2019, **68**, 200-204.

13 Z. Li, C. Liu, J. Guo, X. Zhang, Y. Zhou, L. Shen and W. Guo, *Sol. Energy*, 2018, **171**, 8-15.

14 Z. Li, W. Guo, C. Liu, X. Zhang, S. Li, J. Guo and L. Zhang, *Phys. Chem. Chem. Phys.*, 2017, **19**, 20839-20846.

15 D. Qin, H. Cao, C. Yan, S.-S. Meng, J.-X. Tang and X. Zhan, *J. Mater. Chem. A.*, 2017, **5**, 25385-25390.

16 L. Zhu, B. J. Richardson and Q. Yu, *Phys. Chem. Chem. Phys.*, 2016, **18**, 3463-3471.

17 C. Chen, S. Jin, J. Zhang, Q. Yang and D. Qin, *Thin Solid Films*, 2020, **697**, 137836.

18 J. Subbiah, C. M. Amb, I. Irfan, Y. Gao, J. R. Reynolds and F. So, *ACS Appl. Mater. Interfaces*, 2012, **4**, 866-870.